An innovative method to identify structural change through ion-molecule collision, making use of Time-Of-Flight measurements and SIMION simulations.

Nicolas Solem, Claire Romanzin, Christian Alcaraz, Roland Thissen

Received: 15 December 2023 | Revised: 6 May 2024 | Accepted: 23 May 2024

DOI: 10.1002/jms.5066

RESEARCH ARTICLE

Proceedings of the 39th Informal Meeting on Mass Spectrometry

Journal of MASS SPECTROMETRY WILEY

An innovative method to identify structural change through ion-molecule collision, making use of Time-Of-Flight measurements and SIMION simulations

Nicolas Solem | Claire Romanzin | Christian Alcaraz | Roland Thissen

Université Paris-Saclay, CNRS, Institut de Chimie Physique, UMR8000, Orsay, 91405, France

Correspondence
Roland Thissen, Université Paris-Saclay, CNRS, Institut de Chimie Physique, UMR8000, 91405 Orsay, France.
Email: roland.thissen@universite-paris-saclay.fr

Abstract

Structural change of ions induced by collision with a neutral has been studied in a guided ion beam tandem mass spectrometer, using Time-Of-Flight measurements and SIMION simulation. The exothermic catalytic isomerization of HOC^+ to HCO^+ is used to explore the new methodology. Isomerization is catalyzed via a proton transport mechanism through the interplay of a neutral molecule, the catalyst. Four different potential catalysts, Ne, D_2, CH_4, and $C^{18}O$, were studied at different collision energies. SIMION simulation of the ion path and collision in the instrument leads to the highlight of a specific signature related to the catalytic isomerization in the time-of-flight spectra. This signature is used to identify the experimental conditions where isomerization takes place. Only $C^{18}O$, at low collision energies, gives a clear signature of catalytic isomerization, and a quantitative estimate of the catalyzed isomerization cross-section and rate constant is derived. This new methodology is sensitive to clear presence of catalyzed isomerization and can be used in instruments designed for cross-section measurements, provided low collision energy is used and ion bunching is available.

KEYWORDS
ion-molecule reaction, isomerization, proton transport, SIMION, time-of-flight

1 | INTRODUCTION

Mass spectrometry is inherently insensitive to structure and must be combined with other methods in order to produce structural information. One of the major strategies to this end is to induce the dissociation of the desired ion. The dissociation can be induced either by ionization itself[1,2] or by further activation of ions, such as collision.[3,4] Reactivity also offers the possibility to differentiate isomer ions.[5–8]

Beyond structural determination, probing the structural change, from one isomer to another, is a difficult task in mass spectrometry. If the two isomers have different reactivity or dissociation patterns, it is possible to measure the modification of behavior from the pattern of ions produced after isomerization is triggered, and thus deduce the occurrence of a structural change. This process requires a transition state lying higher in energy than the highest isomer. It results in an isomerization barrier that can be overpassed by collision with a neutral target, either bringing internal energy through collision energy or, and this is the mechanism of interest here, lowering the isomerization barrier in the collision intermediate. In the latter case, the neutral target acts as a catalyst.[9–17]

Catalyzed isomerization by proton transport was first observed by Wagner-Redecker *et al.* in 1985[9] and Freeman *et al.* in 1987[10] in the HOC^+/HCO^+ system, with H_2 as the neutral target acting as the catalyst. However, they did not identify the mechanism leading to the

isomerization. It was first described by Ferguson in 1989[13] and the terminology of catalytic isomerization by proton transport was proposed by Bohme in 1992.[18] Proton transport operates, in the HAB^+ molecular ion (being higher in energy than its ABH^+ isomer), through a two-steps mechanism: (i) first a proton transfer from the A site of the AB moiety to the molecule M, (ii) second a proton transfer from the protonated molecule M to the B site of the AB moiety. Formally, the neutral target M transports the proton from one site to the other, lowering the isomerization barrier, without being modified in the process. In order to have an efficient proton transport, the proton affinity of the catalyst must range between those of the two sites considered in the structural change, A and B.

It is to be noted that the situation is a bit more complex when the neutral target M is either molecular hydrogen or a hydrogenated species. Indeed, in that case, the two steps might consist of a single concerted mechanism where the proton is formally transferred to the neutral target, while another proton from the neutral target is transferred to the AB moiety. This mechanism does not formally correspond to a proton transport and therefore cannot be accounted as isomerization.

The proton transport mechanism has been evidenced on larger molecular edifices and is involved in the catalytic keto-enol[14–16] and formic acid[17] isomerization, with different polar molecules as catalysts. This catalytic isomerization process was mostly studied, in mass spectrometers, using the reactivity or dissociation strategy. We here propose a new methodology to probe the proton transport.

The HCO^+ and HOC^+ isomers, hereafter referred to as CHO^+ generic term, are separated by 1.7 eV, HOC^+ being the less stable isomer. The isomerization of HOC^+ to HCO^+ is restricted by a barrier of 1.5 eV[19] and can be catalyzed by the presence of a neutral molecule,[9–12,19–21] using the proton transport mechanism[18,19] described above. It has been shown, both theoretically[12,19–21] and experimentally,[9–12] that the barrier of the catalyzed isomerization of HOC^+ is inversely proportional to the proton affinity of the neutral collider. The barrier becomes submerged when the proton affinity of the catalyst is higher than the one of the oxygen atom of CO. Proton transfer, to the neutral target, becomes the favored path when the neutral partner has a higher proton affinity than the carbon of CO.

Beyond the physicochemical interest, both CHO^+ isomers have been detected in diverse regions of the interstellar media, such as Photon-Dominated Regions,[22] interstellar clouds,[23–25] or Mars ionosphere.[26,27] The $[HCO^+]/[HOC^+]$ detected ratios are in the range of 20 to 1800.[22–25] This means that HOC^+ can be, unexpectedly, abundant in some environments, HCO^+ being one of the most abundant molecular ions in the interstellar media.[28,29] In order to understand the evolution of these two species and their impact on the formation of complex molecules, it is of great interest to study their reactivity. For HOC^+, isomerization can act as a destruction path. It is, therefore, relevant to describe and quantify it.

Proton transport from HOC^+ to HCO^+ has been studied here, using an innovative Time-Of-Flight (TOF) methodology, inside a tandem guided ion beam instrument. This methodology combines the use of experimental TOF measurements, hereafter referred to as X_TOF, with TOF simulation, hereafter referred to as S_TOF, performed using the SIMION software, to interpret the results. Comparison between the experiments and the simulation highlights a specific signature related to the presence of catalyzed isomerization of HOC^+.

2 | INSTRUMENT AND METHODS

2.1 | Experimental measurements

The experiments were done with the CERISES instrument[30] associated to the DESIRS[31] beamline of the synchrotron SOLEIL. This beamline produces VUV photons in the 5–35 eV range. The CERISES instrument makes use of the VUV photons to produce, by dissociative photoionization, mostly singly charged cations. This set-up is a guided ion beam tandem mass spectrometer, composed of two octopoles located between two quadrupoles mass filters in a QuadI-OctI-OctII-QuadII configuration. The collision cell is a metallic cylinder of 40 mm, in effective length, perforated at both ends by 11 mm diameter apertures. It is located at the end of OctI (Figure 1). Initial kinetic energy of the ions, related to the potential difference of the source and OctI, was determined using the retarding potential method as illustrated in Figure S1.[32] By convenience, the retarding voltage in the following and in figures is the opposite of V_{OctI}. The kinetic energy of ions can be varied in the range 0–20 eV in the laboratory frame, by changing by a same amount the potential of all the elements between the first octopole, included, and the detector. Conversion to the center-of-mass (CM) frame is made to produce comparable results when considering different neutral targets.

The CERISES set-up has been designed with two octopoles in order to describe the kinetic energy released during the reactive collision. The first octopole is 15 cm in length and the second one is 45 cm in length. OctII is set at a potential slightly attractive (−0.7 V) compared to the collision cell (first octopole) in order to allow for ions with slight differences in speed to exhibit measurable differences in their time of flight to the detector. It was therefore proposed to take advantage of this characteristic to witness the kinetic energy released in the catalytic isomerization. To this end, TOF measurements of the $m/z = 29$ HOC^+ parent ions are recorded, using different kinetic energy of the parent ions, to study the effect of a neutral target on the kinetic energy distribution of the ions.

In order to record the time of flight of the ions in the instrument, it is necessary to generate bunches of ions from the continuous flow emerging from the photoionisation source (the nominal repetition rate of SOLEIL, when we performed the measurements, was 352 MHz). Therefore, we had to design a gating procedure in order to repel all ions on their path to the collision cell, except for a limited time, that would correspond to the start of a bunch of ions. To this end, and considering that the HOC^+ ions are produced by dissociative photoionization, it was decided to bunch the ion flow after the mass selection in order to avoid unexpected charging effects induced by the deflection of large ionic currents on insulators. As there is an Einzel lens focalizing ions emerging from the first quadrupole into the first

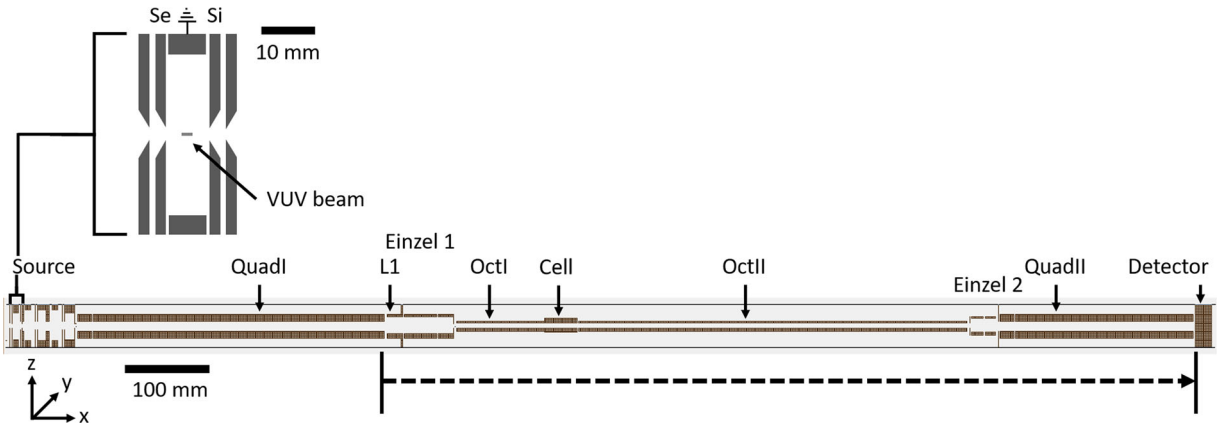

FIGURE 1 Scheme of the CERISES instrument (side view), as reproduced in the SIMION software. The dashed arrow corresponds to the travel of ions considered for the TOF measurements. In the top left is a zoom of the source region. The grey rectangle in the zoom represents the light beam.

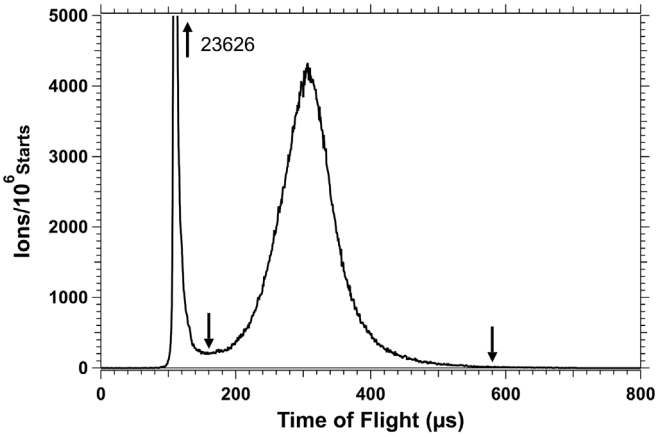

FIGURE 2 Experimental TOF spectrum without gas in the cell. The collision energy in E_{LAB} is 0.2 eV. The sharp peak is an artefact, and the broad one is the peak of interest. The two arrows indicate the time range, which is used for further treatments.

octopole, a digital pulser (Agilent 33220A, 20 MHz) was connected to the first element of this lens (L1, Figure 1). The potential of this 2 cm long cylindrical electrode giving optimal transmission of the lens is equal to −2.8 V. Bunches of ions were generated at a frequency of 1 kHz by applying a default value of +10 V (gate closed) on that element, and lowering the value at −2.8 V (gate opened) for a duration of 10 µs. In these conditions, counting rates of about 1,000 ions.s^{-1} were measured. On average we aimed at the recording of an integral of 1 million ions, representing roughly 15 minutes of acquisition per X_TOF spectrum.

Thanks to the retarding potential method, it is possible to slow down ions in the CERISES instrument to very small speeds. Therefore, flight times up to 2 ms can be recorded. The Data acquisition module used for this purpose is a National Instruments PCI 6602 DAQ, which was operated at a time resolution of 0.8 µs, and used the digital pulser trigger signal as start of its measurements. An X_TOF spectrum can then be generated and corresponds to the histogram of all individual flight times recorded during the acquisition. Since these flight times are measured between the opening of the gate and the detection of the ion by the detector (Figure 1), it corresponds to the travel time of the ions in this part of the instrument.

A typical X_TOF spectrum is shown in Figure 2. It is composed of two peaks: (i) a sharp artefact at short time (∼100 µs) and (ii) the peak of interest (between 150 and 600 µs). (i) The artefact is a consequence of the length of the pulsed element used to generate the ion bunch. When L1 is set back to +10 V, the ions still present in L1 will be artificially set at the upper potential. This will result in an important kinetic energy increase for these ions, when exiting L1, and lead to the formation of a peak at short time, the artefact. (ii) The peak of interest corresponds to the travel time of the ions inside the CERISES instrument between the end of the first quadrupole and the detector. The maxima of both peaks are shifted with the retarding voltage applied. This effect is more important for the peak of interest than for the artefact. Since the kinetic energy of the ions is proportional to the retarding potential applied, there will be a decrease of resolution of the initial kinetic energy distribution, resulting into a sharpening of the peaks.

Target gases were introduced in the collision cell. Absolute pressures were measured using a MKS398H differential manometer (baratron gauge). The pressure was kept below 160 nbar, in order to ensure the single collision regime, with a maximum of 10% of the parent ion attenuation. Because the collision cell has apertures at both ends, the neutral target gas will constantly flow out. This escaping gas may interact with parent ions outside the collision cell, in regions of the instrument where ions have different kinetic energies. It adds an undesired contribution to the results. In order to remove this background contribution, identical measurements are performed with an identical flux of neutral gas introduced in the chamber surrounding the collision cell. The differences between the two measurements, the one with gas in the cell and the one with gas in the chamber, thus correspond to the actual reaction occurring inside the cell.[33] The same

TABLE 1 Relative proton affinities (ΔPA = PA(X) – PA (CO*) with CO* the proton affinity of the oxygen of CO), catalyzed isomerization barrier from HOC^+ to HCO^+, experimental collision energies in the center of mass frame (E_{CM}), suppliers, purities and working pressures for the different neutral targets used. ΔPA and barrier values are taken from (a) Chalk and Radom,[19] (b) Herbst and Woon[20] and (c) Fridgen and Holmes.[12]

Target	ΔPA (kJ·mol−1)	Barrier (kJ·mol−1)	Barrier (eV)	E_{CM} (eV)	Supplier	Purity	Pressure (nbar)
$Ne^{(a)}$	−228.3	131	1.36	0.33	Air liquide	N50	145
				0.49			
$D_2^{(b)}$	−7.8	−2.9	−0.03	0.10	Air liquide	N27	150–160
				0.20			115–125
				0.40			
				0.78			
$CH_4^{(c)}$	113.4	−106	−1.10	0.08	Alphagaz	>99.99%	40–45
				0.10			68–70
				0.16			
				0.30			
				0.45			
				0.59			
$C^{18}O^{(a)}$	158.1	−163	−1.69	0.11	Aldrich	Isotopic: 95%	45–52
	0	−10	−0.10	0.14		Chemical: 99%	47–75
				0.24			
				0.44			

methodology will be used here after to witness the catalytic isomerization process in the cell.

HCO^+ and HOC^+ were produced via dissociative photoionization using respectively: formaldehyde (H_2CO)[34,35] and deuterated methanol (CD_3OH).[36,37] The reactivity of HCO^+ and HOC^+, as a function of photon and collision energies, were studied during the same measurement session but are not presented here. HOC^+ is known to appear at a photon energy of 14.8 eV, from the dissociative photoionization of CD_3OH.[37] Differential charge transfer reactivity of HCO^+ and HOC^+ allowed us to demonstrate that the population of $m/z = 29$ formed from the CD_3OH precursor contains roughly ~90% of HOC^+ at a photon energy of 18 eV.[38] This photon energy was selected using both the undulator and monochromator of the DESIRS beamline. The exit slit of the monochromator was set at 600 μm during all the experimental measurements. Second order light from the undulator was removed using the DESIRS gas filter[39] filled with neon.

Four different neutral targets were studied as potential catalysts: $C^{18}O$, CH_4, D_2 and Ne. They were chosen because of their proton affinity that provide a diversity of behaviors of the catalyzed isomerization barrier. Details are given in Table 1. $C^{18}O$ is used in order to avoid mass overlap between the isomerization and the proton transfer products.[40,41] Increasing collision energy could increase the ability to do the isomerization as there will be more energy available to overcome the barrier, yet this effect will compete with the decreasing probability of forming a complex (illustrated in the upper part of Figure S1).[42,43] Different collision energies were used for each target to investigate the impact of these two effects.

The deuterated methanol was bought from Euriso-top and had an isotopic purity above 99.5% and a chemical purity above 99%. For the other chemicals, provider and purity are indicated in Table 1.

2.2 | Simulation of time-of-flight spectra

SIMION® is a software that simulates charged particles' behavior inside electrostatic and magnetic fields.[44] SIMION 8.0 was used to simulate the travel time of singly-charged ions, of mass 29, inside a reproduction of all the electrodes and elements of the CERISES instrument, with a cylindrical symmetry (Figure 1). In order to simulate the experimental results, two specific codes were developed for (i) ion generation and (ii) gating and collision simulation.

The two codes were developed using Lua, one of the scripting languages of SIMION. The 32 elements simulating the CERISES instrument were set at the same potentials as in the experimental measurements. The most important ones are summarized in Table 2. The radiofrequency oscillations of the potential applied on the quadrupoles and octopoles were not simulated. Instead, when flying in those elements, the ions were artificially kept on the x axis of the simulation at every time step. However, the kinetic energy and orientation of ions was maintained at the fixed values they had at the entrance of the element, so that their y and z positions became free again when exiting the elements. When operated as mass selectors, fringe field effects in the quadrupole filters have an impact on the kinetic energy of the transmitted ions.[45] In order to mimic this effect for the first quadrupole it appeared necessary to add a random kinetic

TABLE 2 Potentials used in the SIMION simulation for the CERISES instrument. The values are in Volt. Se and Si electrodes define the extraction field inside the 8 mm width ion source. The potentials of the elements and electrodes in the second line are floating according to the variable retarding potential. (a) The two values for L1 correspond, respectively, to the potential when the gate is opened or closed. The Einzel lenses 1 and 2, from Figure 1, correspond to the electrodes marked (b) and (c), respectively.

Se	Source	SI	QuadI	L1[(a,b)]	L2[(b)]	L3[(b)]	
+0.4	0	−0.4	−2	−2.8/+10	−29.36	−0.67	
OctI	**OctII**	**8Pex[(c)]**	**Q1[(c)]**	**Q2[(c)]**	**Q3[(c)]**	**PrefQII**	**QuadII**
0	−0.7	0.376	−2.4	−499	−76	−24	−2.4

TABLE 3 Distributions of the different parameters describing the formation of the ions in the simulation, with x, y and z as defined in Figure 1.

Parameter	x position	y position	z position	Orientation	Initial speed
Distribution	Gaussian FWHM = 1 mm	Uniform width of 2 mm	Uniform width of 0.6 mm	Uniform 4π steradians	Maxwell-Boltzmann at 300 K

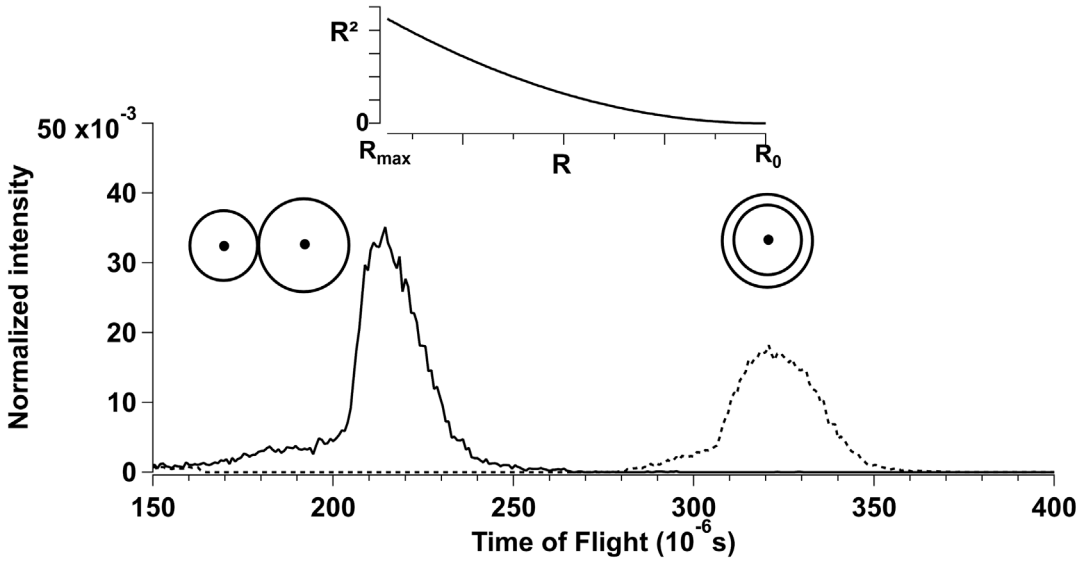

FIGURE 3 Simulated TOF for the head-on collision (dashed line) and the long-distance interaction (full line). The top curve illustrates the R^2 factor applied when interpolating between the two conditions. The circles schematize the long-distance interaction (left), or the head-on collision (right). For long-distance interaction, the neutral and ion have their centers separated by R_{max} and for the head-on collision both centers are in R_0.

energy, between −0.25 eV and 0.25 eV, to the x kinetic energy, as illustrated in Figure S2.

The generation of the ions was simulated stochastically from the center of the source with distributions mimicking the experimental ones. This includes initial kinetic energy distribution according to a Maxwell-Boltzmann distribution, at 300 K, and reproduction of the ion 3D formation zone resulting from the overlap between the projection of the hole in the SI electrode, 2 mm in diameter, and the VUV beam emerging from the DESIRS beamline (Table 3). The distribution along the z axis is uniform because the exit slit of the monochromator was opened at 0.6 mm and is imaged at its focal point in the center of the ion source of the instrument with a uniform flux of photons.[31]

In order to simulate the collision, two extreme cases were considered, both in the hard-sphere model: (i) a tangent long-distance interaction (R_{max}) and (ii) a head-on collision (R_0) (Figure 3). These two extreme cases were considered as approximations to simplify the energy partition between the ion and the target at the moment of the collision. (i) For the R_{max} case, no kinetic energy partition between the ion and the target is considered. This case corresponds to the ion and the target getting close to one another but not colliding. On the opposite, (ii) the R_0 case corresponds to the ion and the target colliding with their centers aligned. The target is considered to be at rest before the collision. In this case, the one-dimension equation for an elastic collision is assumed, inside the CM frame:

$$u'_{ion} = -u_{ion} \quad (1)$$

with u referring to the speed in the CM frame before the collision, u' to the speed in the CM frame after the collision.

In the simulations, all ions collide and all collisions lead to isomerization, when considering exothermic interaction. Approximation of a long-lived complex is considered, so that the kinetic energy released in isomerization will be released in any direction. According to Wagner-Redecker *et al.*,[9] the formed HCO^+ has very low internal energy after proton transport catalyzed by H_2. We therefore consider that all the exothermicity of the isomerization is converted into kinetic energy.

The S_TOF spectra are discreet histograms, where each point is separated by 0.8 μs, as in the X_TOF spectra. It appears that S_TOF spectra, for both extreme cases, are very similar in shape but shifted in time, with the head-on collision case being at longer time (Figure 3). This demonstrates that the distribution of impact position (R) is essentially changing the travel time of the ions and not the shape of the distribution. It is therefore possible to interpolate all the intermediate conditions of collision from the two extreme cases, R_0 and R_{max} collisions. As it is less probable to hit a target in the center than at its periphery, a factor proportional to R^2 (the surface on the sphere), was used (Scheme and inset curve in Figure 3).

In the simulations, CH_4 was used as a proxy of the neutral target. This choice was led by the lighter mass of CH_4, $m/z = 16$ u, compared to the ion, $m/z = 29$ u, so that the final speed of the ion will be, most of the time, positive in the laboratory frame after the collision. It allows for most ions to reach the detector, and have better statistics in the same amount of time than if $C^{18}O$ was chosen. Between $7x10^5$ (for the athermic interaction simulation) and $2x10^6$ (for the exothermic interaction simulation) ions were launched in each simulation.

3 | RESULTS

3.1 | Experimental measurements

The X_TOF spectra of $m/z = 29$ ions were measured with four neutrals: Ne, D_2, CH_4 and $C^{18}O$. Those targets were chosen according to their proton affinity, and their associated ability to lower the isomerization barrier between HOC^+ to HCO^+. The thermodynamic data and the collision energies used are summarized in Table 1. $C^{18}O$ has either the same proton affinity or an higher proton affinity than the oxygen of CO, so the barrier is submerged and the isomerization should be possible.[19] CH_4 has a proton affinity between the one of the oxygen and the carbon of CO. The isomerization barrier is also submerged.[12] H_2 and Ne have lower proton affinity than the oxygen of CO, the barrier is then positive for Ne[19] but for H_2 it is only slightly negative.[20] Similarly to the strategy used for cross-section measurements, measurements were performed with gas in the collision cell and with gas in the chamber outside the cell, in order to record X_TOF spectra in conditions where collision was or wasn't taking place. The cell and chamber X_TOF spectra were very similar. Indeed, to be in the single collision regime, a pressure leading to a maximum of 10% attenuation of the parent ions signal is used, meaning that a very small fraction of ions is undergoing a collision, among which a part only will lead to isomerization. In order to highlight faint effects of the presence of gas in the collision cell, the difference between the two sets of spectra (cell and chamber) has been made. "Cell", the X_TOF spectrum in cell is normalized to, "Chamber", the X_TOF spectrum in chamber in the time range depicted in Figure 2. For this the following equation was used for each time bin of the X_TOF spectrum:

$$\Delta = Cell * \left(\frac{\int peak_{Chamber}}{\int peak_{Cell}} \right) - Chamber \quad (2)$$

This leads to positive signals in X_TOF regions where signal is more important when the gas is present in the collision cell and to negative signals in the opposite case. As differences for individual points in X_TOF are relatively noisy, five iterations of a binomial smoothing were applied on difference datasets and the result is superimposed as continuous line with tones of grey filling (Figure 4). There is a systematic pattern visible in Figure 4, whatever the neutral target; the negative signal occurs at shorter time and is followed by positive signal at longer times. This can be interpreted as due to the fact that the interaction between the ion and the neutral target is slowing down the ions. However, from these sole results no conclusion on the occurrence of isomerization can be drawn.

3.2 | Simulated time-of-flight spectra

Contrary to the X_TOF spectra, the S_TOF spectrum in absence of collision and the one produced by interpolation of the two extreme cases of collisions are very different. This is due to the fact that we considered that all the ions do collide. Adding the exothermicity from the isomerization in the simulation did modify the shape of the peak of interest, splitting the peak into two broad components, one at smaller TOF and one at higher TOF.

Through this, we obtain two sets of S_TOF spectra, simulating either a non-reactive collision (Figure 5, A) or a collision inducing the exothermic isomerization (Figure 5, B) which can then be considered as representative spectra for the process we want to highlight.

Similarly to the processing of X_TOF spectra, the difference between reactive or non-reactive S_TOF spectra and the S_TOF spectrum simulating ions in absence of gas in the cell were calculated after proper normalization (Figure 5). Comparing these differences, a specific signature appears at short times for the difference spectrum, corresponding to exothermic collision (Area 1). This signature is present for every collision energy used in the simulation: 0.035, 0.28, 0.57 and 1.14 eV in the CM. It results from the general shape of the interpolated S_TOF spectrum for the exothermic collision. Indeed, the S_TOF peak separates into two broad components, and it is the component at short TOF that is responsible for the specific signature. As the signature is not present at all for the athermic collision, conclusion can be made that it is a marker of the isomerization. If the isomerization induced by collision occurs in the experiments, a similar signature should be visible in the X_TOF differences. The longer time region of

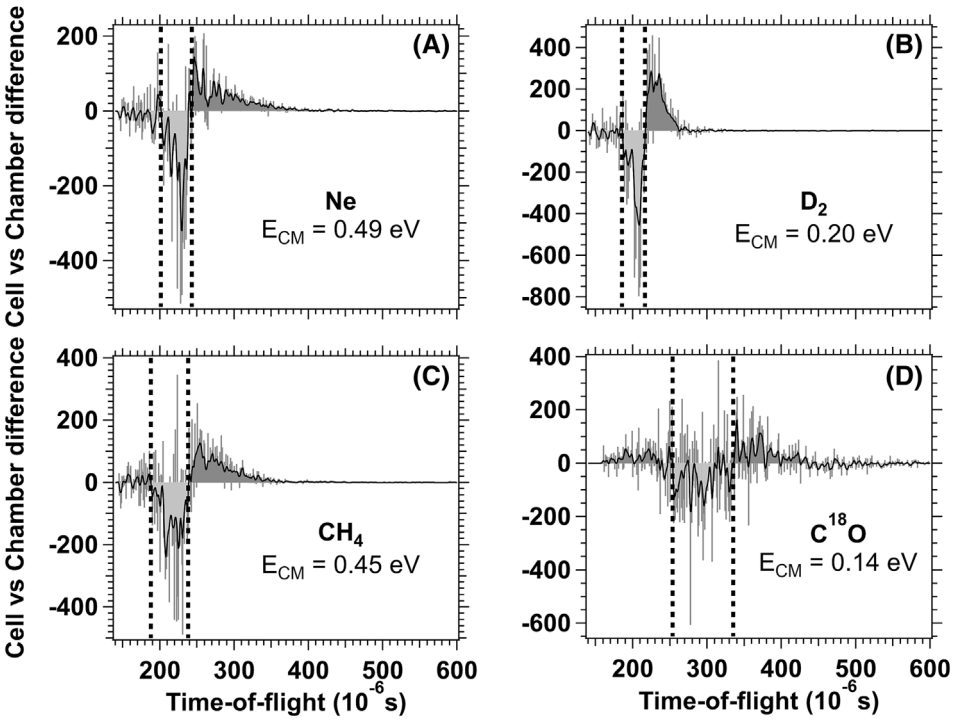

FIGURE 4 Differences of experimental TOF spectra for different neutral targets. A) Ne, B) D_2, C) CH_4, D) $C^{18}O$. For all the measurements, the photon energy used was 18 eV. The dashed lines represent the separation between the three areas. Five binomial smoothing iterations of the differences are shown in continuous lines. The light grey filling corresponds to negative differences, and the darker to positive differences.

the S_TOF differences is also modified when considering the exothermic collision, but the shape at longer time range is not dramatically modified and therefore it would be difficult to ascribe a change of behavior by analyzing only this part of the X_TOF differences.

4 | DISCUSSION

The isomerization signature observed in the S_TOF differences for an exothermic collision, is due to the situations where the exothermicity is released in the forward direction, hence decreasing the travel time of the ions.

In order to perform a quantitative evaluation of the signature for the X_TOF differences, three different regions were identified in the S_TOF difference spectra, and their area was extracted. They are identified in Figure 5. Area 1 corresponds to the signature region that becomes positive when isomerization takes place; Area 2 is always negative and corresponds to the main peak in S_TOF spectrum without gas; and Area 3 is always positive and corresponds to ions that have been slowed down in the collision process or ions that were released backward in the exothermic collision. Comparisons between the area of the three different regions identified in the S_TOF and X_TOF differences spectra have been performed.

The ratio between Area 1 and Area 2 can in particular help identifying the conditions where the isomerization signature is present (Figure 6). Let us consider first the results of the simulations. There is a clear separation between two extreme behaviors, related to the presence (full circle) or absence (full triangle) of the isomerization signature. As Area 1 is only positive when isomerization is present, and Area 2 is always negative, ratios below zero strongly hint at isomerization taking place, while ratios close to zero or slightly positive hint at a minor amount of isomerization. One can notice as well in Figure 6 that there is a loss of sensitivity of the method when increasing the collision energy. It is related to the loss of contrast due to the constant value of 1.7 eV exothermicity, compared to the initial kinetic energy of the $m/z = 29$ ions. However, as we expect catalytic isomerization to involve a long-lived complex, high collision energy is not expected to lead to a strong isomerization signature.

Things get a bit more complicated when it comes to X_TOF spectra.

In principle, one can consider that if an experimental Area 1/Area 2 ratio lies between the two simulations, the amount of isomerization can be derived from the proximity to either trend observed in the simulated result in Figure 6, the negative one corresponding to 100% of isomerization and the positive one to 0%. However, experimental ratios close to 0 can be interpreted in two ways. Either a small amount of isomerization happened, or the difference between the two X_TOF spectra is too noisy. Therefore, the grey dashed zone in Figure 6 corresponds to ratios where it appeared difficult to determine if isomerization is present or not. The experimental points shown in Figure 6 correspond to one to four experimental measurements. When multiple measurements were made, they were averaged. Nevertheless, a general trend can be derived from Figure 6 the ratios corresponding to the four neutral targets seem to be organized between the 100% and 0%, and with ratios at 100% for $C^{18}O$, ratios closer to average with CH_4, ratios slightly positive with D_2 and ratios closest to the 0% isomerization limit with Ne. This general result is in perfect agreement with the anticipated catalytic activity of the targets.

For $C^{18}O$, isomerization is expected as the barrier is always submerged,[19] therefore one can expect negative ratios. The ratios

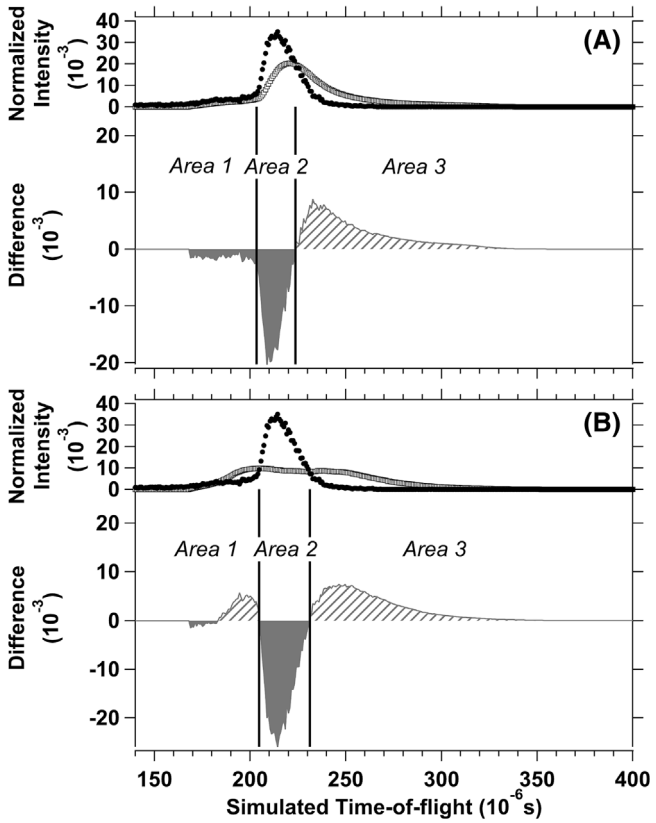

FIGURE 5 Simulation of athermic collisions (A) and exothermic by 1.7 eV collisions (B). In the upper part of both A and B are the simulated TOF spectrum, with open squares for target present and filled circles for target absent. The lower part of both A and B is the differences between the upper simulated TOF spectra. Hatched is where there is more intensity in TOF spectra with gas, and in grey where there is more intensity in TOF spectra without. The datasets were simulated for the neutral target CH_4 and a collision energy of 1.6 eV in the laboratory frame ($E_{CM} = 0.57$ eV).

derived at the two lowest ion collision energies used are close to the simulation curve derived when considering exothermic collisions. This confirms that an important part of the HOC^+ ions do isomerize when $C^{18}O$ is present in the collision cell. Two other collision energies were used for $C^{18}O$ target and they exhibit a ratio close to 0. It may either be interpreted as the fact that there is a lower amount of isomerization compared to the datasets recorded at lower collision energy. This can be related to the expected decrease of the probability of a complex formation when increasing of the collision energy, as described in the Langevin capture model[42,43] and illustrated in Figure S1. Nevertheless, the fact that isomerization occurs, with $C^{18}O$ as the neutral target, is consistent with the strong barrier lowering determined theoretically by Chalk and Radom.[19]

For CH_4, catalytic isomerization is expected to happen, as the barrier is submerged.[12] For this potential catalyst, two behaviors are observed. First, for the lowest collision energy used, $E_{CM} = 0.08$ eV, the TOF spectra is very broad and no Area 3 was observed. As only one measurement was done for this experimental condition, this singular behavior cannot be ascertained. Therefore, the experimental point has been discarded. All the other experimental conditions show Area 1/Area 2 ratios close to 0, but almost always negative. It may mean that the interaction between HOC^+ and CH_4 does form HCO^+, as expected, but to a lower extent than for the two lowest collision energies used for $C^{18}O$. Moreover, as CH_4 is a hydrogenated species, there are two mechanisms to produce HCO^+ from HOC^+. The first one is the catalyzed two-step isomerization, where the hydrogen coming from the oxygen of CO is transferred to the carbon of CO. The second one is the concerted one where the hydrogen transferred to the carbon of CO comes from the methane itself. It is then not the same hydrogen at the beginning and at the end of the reaction on the carbon monoxide. Experimental ratios for CH_4 could be the result of both mechanisms and correspond to an upper limit of the catalyzed isomerization. However, though faint, the presence of isomerization would be consistent with the results obtained in other experimental studies.[12]

For D_2, the barrier is very close to 0 kJ.mol^{-1}.[20] Therefore, catalytic isomerization should take place. The experimental Area 1/Area 2 ratios are close to 0, but almost always positive. Comparing these ratios to the ones obtained for CH_4, they are higher, which formally can be interpreted as that less HCO^+ is formed when using D_2 as the neutral target. With D_2 as potential catalyst, the only mechanism available to form HCO^+ is the catalytic isomerization. This may explain the higher ratios compared to CH_4 that also include the chemistry mechanism. This suspected presence of catalytic isomerization with D_2 as the neutral target is consistent with other experimental studies,[9–11] and with the lowering of the barrier close to 0 kJ.mol^{-1}.[20]

D_2 and CH_4 do not show any real collision energy dependency. Because the barrier for these two neutral targets is submerged, it can be expected that increasing collision energy will not increase the probability to overcome the barrier. As the increase of collision energy is decreasing the probability of a complex formation, as described by Langevin[42,43] and illustrated in Figure S1, a decrease of the probability of the catalytic isomerization is expected. The absence of effect as a function of the collision energy is then in contradiction with this theory. Noisy signals could also account for this apparent absence of collision energy dependency.

For Ne, a positive barrier of 1.36 eV remains.[19] Therefore, isomerization is not expected *a priori*, since additional energy is required to overcome this barrier. Comparing the two collision energies used for measurements with Ne, $E_{CM} = 0.33$ and 0.49 eV, the Area 1/Area 2 ratio is decreasing when the collision energy increases. Yet these collision energies are not sufficient to promote the isomerization. This would imply a substantial amount of internal energy to be present in the HOC^+ ion. Considering that HOC^+ is formed by dissociative photoionisation at 18 eV, and that their appearance energy is 14.8 eV,[37] the HOC^+ ions could have up to 3.2 eV of internal energy, which would then be sufficient. However, this would request for no energy to be imparted in the photoelectron and the 3 deuterium released in the dissociative photoionisation.

The area of the positive signature observed on the S_TOF spectra differences corresponds to 9% (∼ 1/11) of the total area of the S_TOF spectra obtained considering the exothermic collision. From

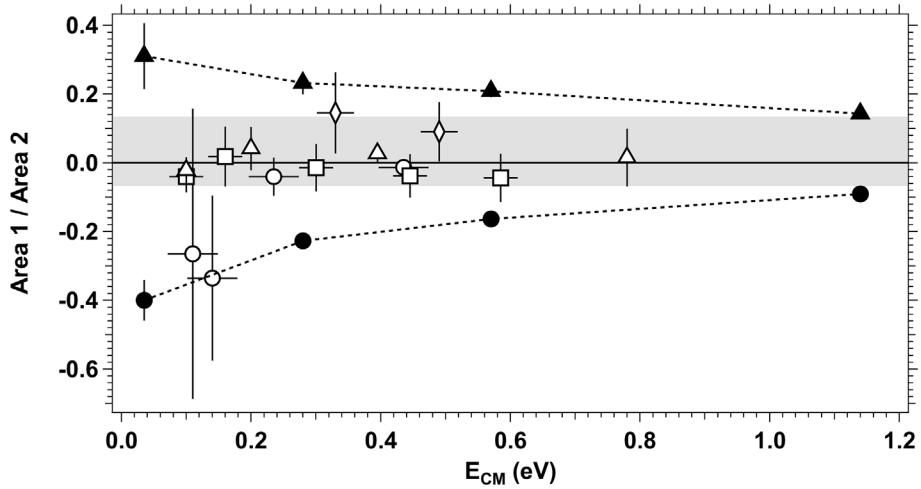

FIGURE 6 Ratio between Area 1 and Area 2, as defined in Figures 4 and 5, for simulated and experimental data. The empty markers correspond to experimental results, while filled markers to simulated results. In experimental results, markers differentiate neutral targets as follows: circles for $C^{18}O$, squares for CH_4, triangles for D_2, and diamonds for Ne. In the simulation with CH_4 as a proxy of the neutral target, triangles correspond to simulation without isomerization and circles to simulation with isomerization. The grey area corresponds to Area 1/Area 2 ratios range where noisy results and presence of little isomerization are difficult to distinguish. Error bars on the ratio Area 1/Area 2 are presented for the simulated and experimental results. Error bars on the collision energies are also presented for the experimental results.

this observation, it is possible to extract the area corresponding to the isomerization from the X_TOF spectra differences where the positive signature is observed and from this, estimate the cross-section for the catalyzed isomerization. The estimate was made on the X_TOF spectrum with $C^{18}O$ recorded at 0.14 eV collision energy (Figure 4, D). The cross-section was calculated with the formula:

$$\sigma = \frac{K}{P}\frac{N_{pro}}{N_{par}} \quad (3)$$

with σ the cross-section in $Å^2$, K a constant of 91,400 $x10^{-29}$ N, P the pressure of neutral gas introduced in the cell expressed in nbar, N_{pro} the number of products, here the area 1 multiplied by 11, and N_{par} the number of parents, here the area of the peak of interest for the X_TOF in chamber.

This estimation leads to a cross-section of ~30 $Å^2$, which corresponds to an efficient process occurring for most of the collisions. From this estimated cross-section, a rate constant for the catalytic isomerization can be derived, using the following equation:

$$k_i = \sigma_i 10^{-16} \langle v \rangle \; with \; \langle v \rangle = \kappa \sqrt{\frac{2}{\mu} E_{CM}} \quad (4)$$

with k_i the rate constant in $cm^3.s^{-1}$, σ_i the cross-section in $Å^2$, $\langle v \rangle$ the average of relative velocities, in the CM frame, of the two collision partners centered on the mean value in $cm.s^{-1}$, κ a conversion constant equal to 9.8 $x10^5$ considering the neutral target at rest in the laboratory frame,[46] E_{CM} the collision energy in CM frame and μ the reduced mass of the ion and the neutral target.

The derived rate constant is $k = 4\ x10^{-10}\ cm^3s^{-1}$, for $C^{18}O$ as neutral target at 0.14 eV of collision energy in CM frame. This result is consistent with values obtained by Freeman et al[10] and Smith et al[11] with H_2: 4.7 and 3.8 $x10^{-10}$ $cm^3.s^{-1}$, respectively. However, the rate constant for the isomerization catalyzed by D_2 seems notably smaller. Indeed, the Area 1/Area 2 ratios for CH_4 and D_2 are closer to 0 while the one for $C^{18}O$ at $E_{CM} = 0.14$ eV is similar to the simulation trend with 100% of isomerization. Therefore, the rate constant estimated here should be rather considered as an upper limit value.

5 | LIMITATIONS OF THE CURRENT METHOD

Results shown in Figure 6 exhibit a general trend that is in good agreement with predicted barrier lowering effects and kinetic energy effects vs capture. However, though we aimed at the acquisition of 1 million ion in the X_TOF measurements, the need to perform differences between spectra to highlight isomerization effects results in the X_TOF spectra differences, which are still quite noisy. Therefore, it can be difficult to differentiate a limited isomerization from a noisy signal. These are synchrotron measurements, and therefore limited time was available to perform the full exploratory program. In addition, to study the catalytic isomerization of HOC^+, with only one partner, we needed to be in the single collision regime. To reach this regime, we need to work with pressure in the collision cell between 40 and 160 nbar. In these conditions, only a small fraction of parent ions interact with the target gas (maximum 10%). Therefore, it limits the intensity of the possible reactions, including the catalytic isomerization. Longer acquisitions time should give access to better statistics and eliminate the possible confusion. Nevertheless, the error bars presented in Figure 6 are quite reasonable and confirm the trends and conclusions.

We have been able to retrieve a quantitative information for the cross section and rate constants, but only for the experimental point corresponding to a ratio similar to the simulation one when considering 100% isomerization. There is a systematic presence of a small, underlying, negative contribution in Area 1 that corresponds to smearing signals interpretable as collision without isomerization. This negative contribution is not constant with the collision energy, and is therefore difficult to quantify and correct for. When the isomerization is small, it renders the determination of cross-section or rate constants impossible.

To obtain the S_TOF, important approximations were made. These approximations simplify the simulation but could impact the accuracy of the results. The approximation of the two extreme cases is valuable considering the S_TOF spectra obtained, but is not reproducing the full variability of impact parameters. For this, the classical mechanics 3D equation for a collision should have been used. However, this would require a considerable increase of parameters to explore that would have largely increase the time of simulations. The hard sphere model used here to simulate the approach of the ion and the neutral target is also a crude approximation of the impact parameter and intermolecular potential. The ion-neutral model of approach would have been more consistent. However, this model is more complex and, again taking it into account would have made the simulations heavy to perform. Another approximation made is the one of the long-lived complex. The proton transport mechanism could take place in complex with shorter lifetime, such as the osculating complex.[47] Nevertheless, as the catalytic proton transport requires two steps, one can expect that the complex leading to this process necessarily exhibits a significant lifetime.

6 | CONCLUSION

The catalytic isomerization of HOC^+ has been studied, making use of TOF measurements inside a tandem guided ion beam instrument and simulations using SIMION. Experimental TOF measurements were recorded, reacting HOC^+ produced by dissociative photoionization of CD_3OH at 18 eV with four neutral targets: $C^{18}O$, CH_4, D_2 and Ne, chosen for their various proton affinities. Different collision energies were used in order to evaluate the opposite effects of energy to overcome the barrier and decreasing lifetime of the capture complex. Experimental TOF measurements with and without gas in the collision cell of the CERISES instrument were done and gave very similar results, requesting for the use of differences of spectra to highlight the effects of interaction with the target gas.

SIMION simulations in a reproduction of the CERISES set-up were performed to highlight a specific signature related to the isomerization process. The interaction between the catalyst and the parent ion was simulated in a hard sphere model, considering two extreme cases: a long-distance interaction (R_{max}) or a head-on collision (R_0). The two simulations were similar in shape but shifted in time, and it was possible to derive all the intermediate approach parameters via an interpolation between these two cases. The approximations of a long-lived complex and a vibrationally cool ion product allowed the 1.7 eV exothermicity of the isomerization to transform into kinetic energy in a random direction. Comparison between athermic interaction simulation and exothermic interaction simulation highlighted a specific signature associated to the isomerization at short time-of-flight.

Three time regions were identified in the simulated time-of-flight difference spectra with alternating positive and negative signals. A quantitative evaluation of the experimental and simulated data was done using the ratio of the area of the specific signature to the area of the most intense negative area. Two experimental conditions are showing a clear presence of isomerization, when using $C^{18}O$ as the neutral target and $E_{CM} = 0.11$ and 0.14 eV. Ratios for other targets or other collision energies are close to 0, either because of noise or a small amount of isomerization. However, a general trend can be derived with the ratios when using CH_4 target closest to the isomerization simulation and the ratios when using Ne target closest to the non-isomerization simulation, in agreement with the anticipated catalytic activity of the targets. A quantitative estimate of the cross-section and rate constant, from the experimental data with $C^{18}O$ at $E_{CM} = 0.14$ eV, gave values, $\sigma = \sim 30$ Å^2 and $k = \sim 4 \times 10^{-10}$ cm^{3}s^{-1}, comparable to other studies of catalytic proton transfer of HOC^+ into HCO^+ by with H_2.

ACKNOWLEDGMENTS

We are grateful to the DESIRS beamline team for assistance during the synchrotron measurements and the installation of the set-up on the beamline, and the technical staff of SOLEIL for provision of synchrotron radiation facilities under project n°20210985.

DATA AVAILABILITY STATEMENT

The data that support the findings of this study are available from the corresponding author upon reasonable request.

ORCID

Nicolas Solem https://orcid.org/0000-0003-4758-1722
Christian Alcaraz https://orcid.org/0000-0002-6816-4664
Roland Thissen https://orcid.org/0000-0003-0916-2594

REFERENCES

1. Shannon TW, McLafferty FW. Identification of gaseous organic ions by the use of "metastable peaks"1. *J am Chem Soc*. 1966;88(21):5021-5022. doi:10.1021/ja00973a045
2. Jerić I, Versluis C, Horvat Š, Heck AJR. Tracing glycoprotein structures: electrospray ionization tandem mass spectrometric analysis of sugar–peptide adducts. *J Mass Spectrom*. 2002;37(8):803-811. doi:10.1002/jms.337
3. Haddon WF, McLafferty FW. Metastable ion characteristics. VII. Collision-induced metastables. *J am Chem Soc*. 1968;90(17):4745-4746. doi:10.1021/ja01019a053
4. Kuki Á, Biri B, Nagy L, et al. Collision induced dissociation study of the major components of silymarin. *Int J Mass Spectrom*. 2012;315:46-54. doi:10.1016/j.ijms.2012.02.021
5. Sefcik MD, Henis JMS, Gaspar PP. The methanium ion, CH5+. Evidence for the structure of a nonclassical ion from reaction studies

by ion cyclotron resonance spectroscopy. *J Chem Phys*. 1974;61(10):4321-4328. doi:10.1063/1.1681738

6. Smith RD, Futrell JH. On the structure of CH5+; a study of hydron transfer reactions from CH4H+ and CD4H+ tandem-ICR. *Chem Phys Lett*. 1975;36(4):545-547. doi:10.1016/0009-2614(75)80300-9
7. Ozturk F, Baykut G, Moini M, Eyler JR. Reactions of the propynylium isomer manifold with acetylene and diacetylene in the gas phase. *J Phys Chem*. 1987;91(16):4360-4364. doi:10.1021/j100300a029
8. McEwan MJ, McConnell CL, Freeman CG, Anicich VG. Reactions of isomeric C3H3+ ions: a combined low pressure-high pressure study. *J Phys Chem*. 1994;98(19):5068-5073. doi:10.1021/j100070a021
9. Wagner-Redeker W, Kemper PR, Jarrold MF, Bowers MT. The formation and reactivity of HOC^+: interstellar implications. *J Chem Phys*. 1985;83:1121-1131. doi:10.1063/1.449474
10. Freeman CG, Knight JS, Love JG, McEwan MJ. The reactivity of HOC+ and the proton affinity of CO at O. *Int J Mass Spectrom Ion Process*. 1987;80:255-271. doi:10.1016/0168-1176(87)87034-9
11. Smith MA, Schlemmer S, von Richthofen J, Gerlich D. HOC+ + H2 isomerization rate at 25 K: implications for the observed [HCO+]/[HOC+] ratios in the interstellar medium. *Astrophys J*. 2002;578(1):L87-L90. doi:10.1086/344404
12. Fridgen TD, Holmes JL. A study of the methane catalyzed isomerization of HCO^+ to HOC^+ and the elimination of methane from metastable Methoxymethyl cation. *Eur J Mass Spectrom*. 2004;10(6):747-754. doi:10.1255/ejms.683
13. Ferguson EE. Reactions of NNOH+ and HNNO+ ions with CH4 and NO. *Chem Phys Lett*. 1989;156(4):319-322. doi:10.1016/0009-2614(89)87100-3
14. Van Der Rest G, Mourgues P, Tortajada J, Audier HE. Gas phase catalyzed keto-enol isomerization of cations by proton transport. *Int J Mass Spectrom*. 1998;179-180:293-300. doi:10.1016/S1387-3806(98)14102-7
15. Van Der Rest G, Nedev H, Chamot-Rooke J, Mourgues P, McMahon TB, Audier HE. "Proton-transport" catalysis in the gas phase. Keto-enol isomerization of ionized acetaldehyde. *Int J Mass Spectrom*. 2000;202(1-3):161-174. doi:10.1016/S1387-3806(00)00242-6
16. Mourgues P, Chamot-Rooke J, van der Rest G, Nedev H, Audier HE, McMahon TB. Catalyzed keto-enol tautomerism of ionized acetone: a Fourier transform ion cyclotron resonance mass spectrometry study of proton transport isomerization. *Int J Mass Spectrom*. 2001;210-211:429-446. doi:10.1016/S1387-3806(01)00447-X
17. Van Der Rest G, Mourgues P, Audier HE. Catalyzed isomerization and decarbonylation of ionized formic acid and dihydroxycarbene. *Int J Mass Spectrom*. 2004;231(1):83-95. doi:10.1016/j.ijms.2003.10.001
18. Bohme DK. Proton transport in the catalyzed gas-phase isomerization of protonated molecules. *Int J Mass Spectrom Ion Process*. 1992;115(2-3):95-110. doi:10.1016/0168-1176(92)85035-X
19. Chalk AJ, Radom L. Proton-transport catalysis: a systematic study of the rearrangement of the Isoformyl cation to the formyl cation. *J am Chem Soc*. 1997;119(32):7573-7578. doi:10.1021/ja971055c
20. Herbst E, Woon DE. Why HOC+ is detectable in interstellar clouds: the rate of the reaction between HOC+ and H2. *Astrophys J*. 1996;463(2):L113-L115. doi:10.1086/310059
21. Vogt-Geisse S, et Toro-Labbé A. The mechanism of the interstellar isomerization reaction HOC+→HCO+ catalyzed by H2: new insights from the reaction electronic flux. *J Chem Phys*. 2009;130:244308. doi:10.1063/1.3147702
22. Fuente A, Rodrıguez-Franco A, Garcıa-Burillo S, Martın-Pintado J, Black JH. Observational study of reactive ions and radicals in PDRs. *Astronom Astrophys*. 2003;406(3):899-913. doi:10.1051/0004-6361:20030712
23. Woods RC, Gudeman CS, Dickman RL, et al. The HCO(+)/HOC(+) abundance ratio in molecular clouds. *Astrophys J*. 1983;270:583. doi:10.1086/161150
24. Ziurys LM, Apponi AJ. Confirmation of interstellar HOC+: reevaluating the [HCO+]/[HOC+] abundance ratio. *Astrophys J*. 1995;455(1):L73. doi:10.1086/309811
25. Liszt H, Lucas R, Black JH. The abundance of HOC^+ in diffuse clouds. *Astronom Astrophys*. 2004;428(1):117-120. doi:10.1051/0004-6361:20041649
26. Fox JL. The chemistry of protonated species in the martian ionosphere. *Icarus*. 2015;252:366-392. doi:10.1016/j.icarus.2015.01.010
27. Matta M, Withers P, Mendillo M. The composition of Mars' topside ionosphere: effects of HYDROGEN: HYDROGEN EFFECTS ON MARTIAN IONOSPHERE. *J Geophys Res: Space Phys Ther*. 2013;118(5):2681-2693. doi:10.1002/jgra.50104
28. Watson WD. Ion-molecule reactions, molecule formation, and hydrogen-isotope exchange in dense interstellar clouds. *Astrophys J*. 1974;188:35. doi:10.1086/152681
29. Watson WD. Interstellar chemistry. *Acc Chem Res*. 1977;10(6):221-226. doi:10.1021/ar50114a005
30. Cunha de Miranda B, Romanzin C, Chefdeville S, et al. Reactions of state-selected atomic oxygen ions O^+ (^{4}S, ^{2}D, ^{2}P) with methane. *J Phys Chem a*. 2015;119(23):6082-6098. doi:10.1021/jp512846v
31. Nahon L, de Oliveira N, Garcia GA, et al. DESIRS: a state-of-the-art VUV beamline featuring high resolution and variable polarization for spectroscopy and dichroism at SOLEIL. *J Synchrotron Radiat*. 2012;19(4):508-520. doi:10.1107/S0909049512010588
32. Teloy E, Gerlich D. Integral cross sections for ion—molecule reactions. I the guided beam technique. *Chem Phys*. 1974;4(3):417-427. doi:10.1016/0301-0104(74)85008-1
33. Armentrout PB. Mass spectrometry—not just a structural tool: the use of guided ion beam tandem mass spectrometry to determine thermochemistry. *J am Soc Mass Spectrom*. 2002;13(5):419-434. doi:10.1016/S1044-0305(02)00347-1
34. Guyon PM, Chupka WA, Berkowitz J. Photoionization mass spectrometric study of formaldehyde H_2CO, HDCO and D_2CO. *J Chem Phys*. 1976;64:1419-1436. doi:10.1063/1.432411
35. Tanaka HK, Prudente FV, Medina A, et al. Photoabsorption and photoionization cross sections for formaldehyde in the vacuum-ultraviolet energy range. *J Chem Phys*. 2017;146:094310. doi:10.1063/1.4977605
36. Berkowitz J. Photoionization of CH_3OH, CD_3OH, and CH_3OD: dissociative ionization mechanisms and ionic structures. *J Chem Phys*. 1978;69:3044-3054. doi:10.1063/1.436995
37. Borkar S, Sztáray B, Bodi A. Dissociative photoionization mechanism of methanol isotopologues (CH3OH, CD3OH, CH3OD and CD3OD) by iPEPICO: energetics, statistical and non-statistical kinetics and isotope effects. *Phys Chem Chem Phys*. 2011;13(28):13009-13020. doi:10.1039/c1cp21015g
38. Article in preparation.
39. Mercier B, Compin M, Prevost C, et al. Experimental and theoretical study of a differentially pumped absorption gas cell used as a low energy-pass filter in the vacuum ultraviolet photon energy range. *J Vac Sci Technol a*. 2000;18(5):2533-2541. doi:10.1116/1.1288196
40. Mladenović M, Roueff E. Ion-molecule reactions involving HCO^+ and N_2H^+: Isotopologue equilibria from new theoretical calculations and consequences for interstellar isotope fractionation. *Astronom Astrophys*. 2014;566:A144. doi:10.1051/0004-6361/201423733
41. Mladenović M, Roueff E. Isotope exchange reactions involving HCO^+ with CO: a theoretical approach. *Astronom Astrophys*. 2017;605:A22. doi:10.1051/0004-6361/201731270
42. Langevin P. Une formule fondamentale de théorie cinétique. *Ann Chim Phys*. 1905;245-288.
43. Tsikritea A, Diprose JA, Softley TP, Heazlewood BR. Capture theory models: an overview of their development, experimental verification,

and applications to ion–molecule reactions. *J Chem Phys*. 2022;157:060901. doi:10.1063/5.0098552
44. Manura, D.J. et Dahl, D.A. (2011). SIMION Version 8.0/8.1 User Manual.
45. Smolanoff J, L/apicki A, Anderson SL. Use of a quadrupole mass filter for high energy resolution ion beam production. *Rev Sci Instrum*. 1995;66:3706-3708. doi:10.1063/1.1146494
46. Nicolas C, Alcaraz C, Thissen R, Zabka J, Dutuit O. Effects of ion excitation on charge transfer reactions of the Mars, Venus, and earth ionospheres. *Planet Space Sci*. 2002;50(9):877-887. doi:10.1016/S0032-0633(02)00063-6
47. Dressler RA, Salter RH, Murad E. Energy partitioning in hyperthermal $O+ + H_2O$ charge-transfer collisions. *Chem Phys Lett*. 1993;204(1-2):111-118. doi:10.1016/0009-2614(93)85613-S

SUPPORTING INFORMATION

Additional supporting information can be found online in the Supporting Information section at the end of this article.

How to cite this article: Solem N, Romanzin C, Alcaraz C, Thissen R. An innovative method to identify structural change through ion-molecule collision, making use of Time-Of-Flight measurements and SIMION simulations. *J Mass Spectrom*. 2024;59(7):e5066. doi:10.1002/jms.5066